Temperature discontinuity at the surface of an evaporating droplet

A. J. H. McGaughey[a] and C. A. Ward[b]
Thermodynamics and Kinetics Laboratory, Department of Mechanical and Industrial Engineering, University of Toronto, 5 King's College Road, Toronto M5S 3G8, Canada

(Received 20 August 2001; accepted for publication 27 February 2002)

In a series of experiments, a temperature discontinuity has been found to exist at the surface of an evaporating water droplet. Statistical rate theory has been used to predict the pressure in the vapor to within the experimental uncertainty during each of the experiments. While the qualitative trend of the D^2 law is observed to be consistent with the measurements, it underpredicts the measured rate of evaporation by 21%–37%. When the temperature discontinuity is taken into account in the D^2 law, the difference between the predicted and measured values is at most 7%. The results suggest that the rate limiting process in the experiments is not diffusion in the gas phase, as is assumed in the D^2 law, but is the interface kinetics.
[DOI: 10.1063/1.1471363]

I. INTRODUCTION

The D^2 law of droplet evaporation[1–4] assumes that the rate limiting process is diffusion in the gas phase. This gas phase model also assumes that the temperature profile across the liquid-vapor interface is continuous. In recent experiments,[5–8] a temperature discontinuity has been measured at a steady, evaporating liquid-vapor interface. The ensuing analysis demonstrated that statistical rate theory (SRT)[9–11] predictions were consistent with the measurements. Based on these results, the possibility of a temperature discontinuity at the surface of an evaporating droplet (an unsteady system) and the relative importance of the interface kinetics on the rate of evaporation in that system have been investigated.

An apparatus has been built in which an evaporating droplet hangs on a thermocouple bead. This allows the measurement of the temperature in the liquid phase during the evaporation process. Along with other system measurements, this permits the construction of a temperature profile in the vapor and the determination of the conditions at the liquid-vapor interface. A temperature discontinuity is found to exist. The results are compared to previous steady evaporation experiments and analyzed using the SRT. The measured rate of evaporation is compared to the predictions of the D^2 law and SRT, and a discussion of the rate limiting process in droplet evaporation is presented.

II. BACKGROUND

A. Droplet evaporation

The D^2 law was the first widely accepted theory developed to model droplet evaporation and combustion. It is a gas phase model that predicts that the surface area of the droplet will decrease at a constant rate given by[12]

$$\frac{dD^2}{dt} = -K, \tag{1}$$

where D is the droplet diameter, t is time, and K is a constant. It models a stationary, single one-component droplet in a gaseous phase which may or may not contain its own vapor in the initial state. In addition to the details given previously, some of the important assumptions are that spherical symmetry exists, convection effects can be neglected, the pressure in the gas phase is constant, the partial pressure of the evaporating species at the liquid-gas interface is equal to the saturation pressure corresponding to the liquid temperature, the transport properties are constant and the liquid temperature is uniform and constant.

From the conservation equations, K is predicted to be[12]

$$K = \frac{8\rho^G \delta^G}{\rho^L} \ln\left(1 + \frac{c_p^G \Delta T}{h_{fg}}\right), \tag{2}$$

where the superscripts G and L refer to the gas and liquid phases, respectively, ρ is density, δ^G is the mass diffusion coefficient of the vaporizing species in the gas phase, c_p^G is the specific heat at constant pressure of the gas phase, ΔT is the difference in temperature between the droplet surface and the ambient gas and h_{fg} is the specific enthalpy of vaporization of the vaporizing species. Law[12] indicates that the estimate of K from Eq. (2) is "crude" and that due to the difficulty in specifying some of the transport properties of the gas phase, the measured value of K is often used as a fitting parameter to set $\rho^G \delta^G$ in experimental analyses. While the predicted value of K may not be useful in all cases, the trend predicted by Eq. (1) has consistently been seen in experimental data. Reviews by Law[12] and Sirignano[13] give a detailed account of the basis of this model, its limitations, and attempts made to improve it.

To try to develop better models, investigators have used different methods to solve the conservation equations which do not make all the assumptions inherent in the D^2 law.[14–20]

[a]Present address: Laboratory for Research in Transport, Reaction and Phase Change in Porous Media, Department of Mechanical Engineering, University of Michigan, 2350 Hayward Street, Ann Arbor, MI 48109-2125.
[b]Author to whom correspondence should be addressed; electronic mail: ward@mie.utoronto.ca

Consideration has been given to factors such as radiation effects,[14] variable thermal properties, nonideal phase behavior,[15] convection effects,[16,17] and separate modeling of the continuum and Knudsen regions.[18]

Very few investigations have considered the possibility of a discontinuous temperature profile across the liquid-vapor interface during droplet evaporation. Young[20] has modeled droplet evaporation and condensation with a temperature discontinuity predicted by the classical kinetic theory (CKT). For evaporation, the temperature in the vapor at the interface is predicted to be lower than that in the liquid. No comparison is made to experimental results. Elperin and Krasovitov[14] develop a droplet evaporation model taking into account the temperature discontinuity proposed by Yalamov *et al.*[21] The temperature discontinuity is shown to affect the late stages of the evaporation process, increasing the predicted total evaporation time of small droplets (diameter $\sim\mu$m) by 10%. The time scale for the evaporation is on the order of milliseconds. There is no known experimental work that has tried to measure a temperature discontinuity at the surface of an evaporating droplet.

B. Temperature profiles near a liquid-vapor interface during evaporation

The conditions existing at a liquid-vapor interface undergoing evaporation are controversial. Specifically, there are different claims as to the nature of the temperature profile near and across the interface. In the past, such a system has been theoretically analyzed using either the continuum approach or CKT. Fang[22] presents a detailed review of this work. There is no known experimental work to support the claims of either of these approaches.

The results of recent experiments[5–8] have questioned the validity of both the continuum approach and CKT. For water evaporating under steady conditions, the temperature in the vapor at the interface was always found to be higher than that in the liquid. Differences as large as 7.8 °C were measured.[5] This difference is also referred to as a temperature discontinuity. For the same experimental conditions, Young's CKT approach[20] predicts a discontinuity of 0.007 °C in the opposite direction. In the experimental work of Refs. 5–8, temperatures were measured to within a few mean free paths of the interface, denying the possibility that the temperature discontinuity predicted by the CKT would only be apparent within the Knudsen layer. Evaporation experiments have also been performed with octane and methylcyclohexane, and similar results were found.[7] The higher temperature in the vapor is interpreted as an indication that it is the higher energy molecules in the liquid that evaporate.[8]

Statistical rate theory can be used to analyze the phase change problem. This theoretical approach is based on the transition probability concept as defined in quantum mechanics and uses the Boltzmann definition of entropy to introduce a thermodynamic description of the system. In the past, the SRT has been applied to rate processes such as gas-solid adsorption,[23–27] permeation in ionic channels in biological membranes,[28] and crystal growth from solution.[29] It can be used to predict that the mass flux across a liquid-vapor interface will be a function of the temperature at the interface in each phase, the pressure in the vapor at the interface and the radius of curvature of the interface.[6] It can be shown that the calculated value of the mass flux is most sensitive to the pressure in the vapor.[7] With this in mind, the expression for the mass flux can be used to predict the pressure in the vapor using the four other known parameters, and this value compared with the experimental measurement. In the experiments of Refs. 5–8, all five of these parameters were independently measured, and good agreement was found between the predicted and measured pressures.

III. EXPERIMENTAL APPARATUS AND PROCEDURES

A. Concept

The objective of the current experimental investigation is to hang a liquid droplet on a thermocouple bead and measure its size and temperature, and the pressure and temperature of the surrounding vapor as the droplet evaporates. Water is chosen as the working fluid. The central component of the apparatus is the test section, a schematic of which is shown in Fig. 1(a). It is a 2.75 in. Conflat flanged double cross as shown in the figure and has a volume of approximately 0.41 L. There are viewing windows on the front, back, and bottom flanges. Through connections to a mechanical vacuum pump (Welch DuoSeal 1400B-80) and a turbomolecular pump (Leybold-Heraeus Turbovac 150) through the left flange, the pressure in the test section can be reduced to 10^{-4} Pa. Water vapor at a desired pressure less than ambient saturation conditions can be introduced to the test section through the left flange without contamination by air. Once an experiment is setup, the test section can be immersed in a water bath with an internal circulator (Lauda MS[H31050]FN) that can maintain the water temperature within ± 0.03 °C.

All thermocouples used in the investigation are of type K (chromel–alumel junction). The thermocouple on which the droplet hangs has an approximately spherical bead with diameter 0.35 mm. A second thermocouple is located 4.30 mm away. These thermocouples will be referred to as the droplet thermocouple and the vapor thermocouple. The diameter of the thermocouple wire is 0.08 mm. The thermocouples are mounted on a linear-rotary motion feedthrough (MDC BRLM-275) that is mounted on the top flange of the test section. A picture of the configuration of the two thermocouples when there is a droplet present in the system is shown in Fig. 1(b).

The droplet is introduced to the system by a needle connected to a syringe that is mounted on a syringe pump (Cole-Parmer 7490-10) that provides fine control of the flow rate (flowrates used were on the order of 10 μL/min). The pump is mounted on a three degree of freedom position manipulator. The syringe can be filled with high purity liquid water from the same source that the vapor is obtained. The needle enters and exits the system through a septum mounted in a 1/4 in. ball valve that is mounted on the right flange of the test section. This setup ensures that there is no significant air leakage at any time. When the needle is inside the test section, it can be isolated from the syringe by a 1/16 in. ball valve and pumped down to vacuum conditions along with

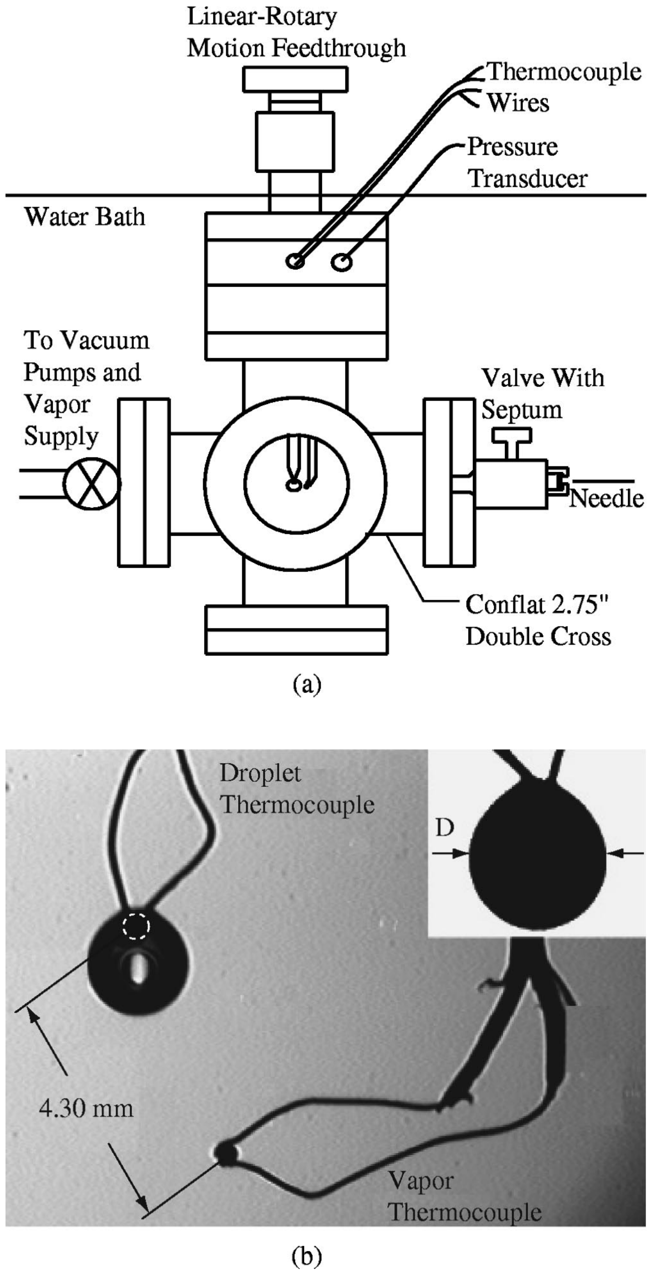

FIG. 1. (a) Schematic of the test section. (b) The configuration of the droplet and the droplet and vapor thermocouples. The main image was taken with a fluorescent light as backlighting. The dashed white circle inside the droplet indicates the location of the thermocouple bead. The inset image was taken with the lighting setup. This is the image used to measure the droplet size.

the test section while the syringe remains full of water. When a droplet is to be formed on the needle, the valve between the needle and the syringe is opened and the pump is advanced until a suitably sized droplet forms on the needle tip. The droplet is transferred from the needle to the droplet thermocouple by adjusting their positions using the feedthrough and the position manipulator. The initial diameter of the droplet is typically between 1.5 and 1.7 mm.

B. Measurements

Measurements of the temperatures read by the droplet thermocouple, the vapor thermocouple and a thermocouple in the surrounding water bath are made using a data acquisition system (HP 39702A connected to an Apple IIci computer running Labview). The thermocouples were calibrated using a mercury thermometer with 0.1 °C divisions that was calibrated against a National Institute of Standards and Technology traceable Okazaki Pt 100 AS7885 RTD temperature probe. The thermocouples are referenced against an ice point (Omega TRC-111). Based on the calibration, the absolute error associated with the measurements is ± 0.1 °C and the relative error between measurements is ± 0.05 °C. The temperatures encountered in the experiments are between 19 and 27 °C. The pressure is measured with a pressure transducer (Omega PX811-005AV) that is also connected to the data acquisition system. The transducer was calibrated against a mercury manometer (inside diameter of 8.0 mm, maximum impurity 5 ppm) using a cathetometer (PTI2212). The zero level of the manometer was verified by pumping down on it with the turbomolecular pump to 10^{-4} Pa. In this configuration, there was no measurable difference between the two column heights. Based on the calibration, the error associated with the pressure readings is ± 20 Pa. The pressures encountered in the experiments are between 2000 and 3300 Pa. A series of tests run with the test section fully evacuated showed that any leakage effects are on the order of the uncertainty in the pressure measurement.[30] It will therefore be assumed that the test section contains only water. The droplet is observed through the front and back viewing windows and its size is measured using a solid state video camera (Cohu 4815-5000/000, with a Canon FD 10014.0 Macro Lens and Kenko No. 4 close up lens) that is connected to image processing software (NIH Image[31] running on an Apple Quadra computer). Light is provided by a small bulb and passes through a collimator (Melles Griot 25 mm) before illuminating the droplet. The image is calibrated using the diameter of the cylindrical rod on which the thermocouples are mounted. The error associated with the droplet size measurements is ± 0.04 mm. A typical image of a droplet used to make a measurement is shown in Fig. 1(b). In the ensuing analysis, the droplet is assumed to be spherical with a diameter taken as the largest horizontal dimension that can be measured. To quantify the effect of gravity on the droplet shape, the surface area was calculated using data extracted from the image. For horizontal diameters between 1.00 and 1.50 mm (the range used in the analysis), the calculated value was at most 5% larger than the area of a spherical droplet with a diameter equal to that measured.

C. Procedure

The water used in the experiments was prepared by passing it through a Barnstead high purity demineralizer cartridge, distilling and de-ionizing with a Barnstead NANOpure water purification system. It was placed in a clean glass vessel and degassed using the mechanical vacuum pump for at least 12 h and then isolated. This vessel was the source of both liquid and vapor. Depending on their composition, all solid components were initially cleaned with a series of acetone, detergent, and chromic acid solutions.

TABLE I. Comparison of the three evaporation tests. Note that the water saturation pressure for a temperature of 26.87 °C is 3540 Pa.

Test	Pressure at $D=1.50$ mm (Pa)	Total evaporation time (s)	Time for evaporation from 1.50 to 1.00 mm (s)	K (10^{-4} mm^2/s)	T^B (°C)
1	3200	13 080	8670	1.49	26.78
2	2880	6870	4200	2.96	26.87
3	2250	3720	2160	5.64	26.80

To prepare for an experiment, the valve between the syringe and the needle was closed, the needle was placed inside the test section, and the system was pumped down with the turbomolecular pump to 10^{-4} Pa for at least 12 h. This was done to remove any contamination that may have entered the system, and to desorb water from the solid surfaces. The syringe was filled with liquid water from the degassing flask. Water vapor was then introduced to the test section, and a droplet was formed on the needle and placed on the droplet thermocouple. It is crucial that the droplet be the only liquid phase in the entire system, and this was verified by observation through the viewing windows. The test section was immersed in the water bath, and the pressure reduced to a predetermined level by pumping with the vacuum pump. When this pressure was reached, the test section was isolated and the evaporation process was observed. Temperature and pressure measurements were begun at ten seconds intervals. The droplet size was measured at a time interval suitable to the rate of evaporation of a given experiment.

IV. RESULTS

A. Droplet size

For the three tests to be considered, the initial droplet diameters were in a range of 1.55–1.70 mm. In order to compare the three tests, the size history will be considered starting at a diameter of 1.50 mm. The pressures at the start of the observation period, which are the key distinction between the three tests, are given in Table I. The time histories of the square of the droplet diameter for the three tests starting at a diameter of 1.50 mm are shown together in Fig. 2. For tests 1 and 2, the droplet size was measured every 3 min. For test 3, the droplet size was measured every 2 min. The data are only plotted up to a diameter of 0.90 mm, where it was found that the droplet shape was no longer spherical due to the effect of the thermocouple bead. Also shown on the graph are best fit lines for each test. As would be expected, the rate of evaporation increases as the initial pressure in the vapor is decreased. Some of the important parameters for the three tests are presented in Table I. The parameter K is the magnitude of the slope of the best fit line through the data, and corresponds to the parameter used in the Eq. (1). The regression parameter provided by Microsoft Excel was greater than 0.997 for all three tests. As the droplet evaporates its weight decreases, causing it to move up the thermocouple wires as the solid-vapor surface tension force becomes more important relative to gravity. At all times between diameters of 1.50 and 0.90 mm, the thermocouple bead was fully submerged in the droplet.

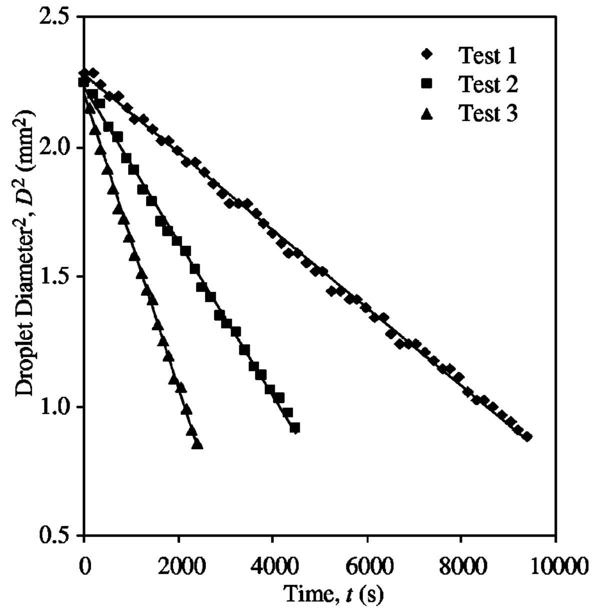

FIG. 2. The time history of the square of the droplet diameter for the three tests. Beyond the last plotted point the droplet was no longer spherical. A linear fit for each data series is included in the plot.

B. Temperatures and pressure

The measured temperature histories for test 2 are shown in Fig. 3(a). The data are plotted for the entire evaporation process and approximately 1000 s afterwards. Relative error bars are included near the beginning and end of the data. When there is still liquid present on the droplet thermocouple, its temperature is always measurably less than the temperature in the vapor, which is always measurably less than the bath temperature. The differences between the three temperatures increase with the evaporation rate (i.e., from test 1 to test 2 to test 3). As the evaporation takes place, both the liquid and vapor temperatures increase. The rate of this increase also rises with the evaporation rate. The temperature profile in the vapor is such that heat is being transferred towards the droplet, in the opposite direction of the mass flux due to the evaporation. The temperature in the vapor increases because the droplet temperature is rising, but also because the liquid surface is receding. The distance between the vapor thermocouple and the droplet surface increases with time, and it will therefore be at a different place in the temperature profile at every instant. It is not until the droplet has completely evaporated that the temperature in the test section rises to the bath temperature. This point is clearly seen in Fig. 3(a) as where the droplet thermocouple temperature rises rapidly. After this time, there is no measurable difference between the three temperatures.

The pressure history for test 2 is plotted in Fig. 4. The trends observed in tests 1 and 3 are similar. As the droplet evaporates, the pressure in the system increases. The total amount of this increase decreases as the evaporative flux decreases (i.e., as the initial pressure increases). The effect of

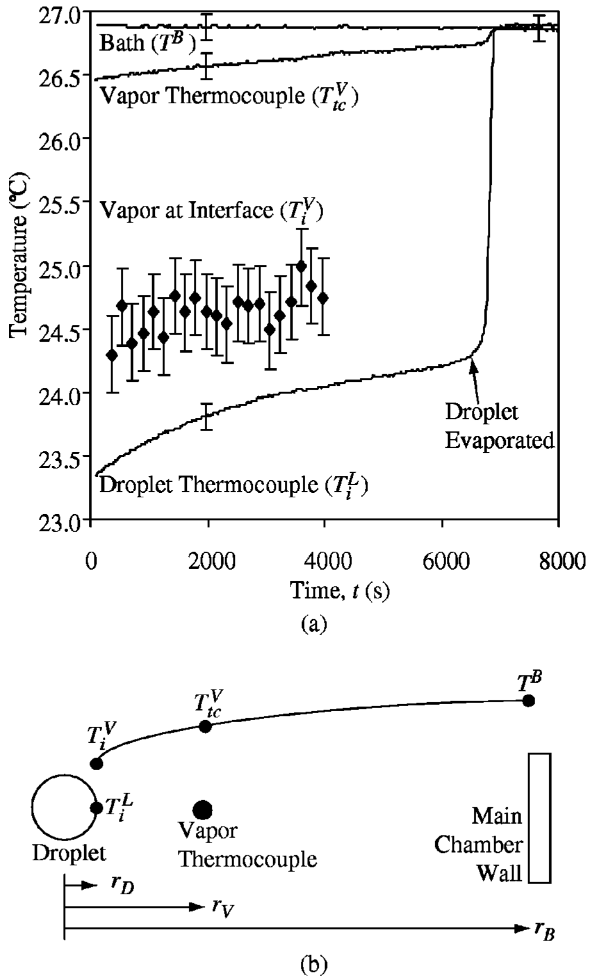

FIG. 3. (a) The temperature histories for test 2. Included are the measured values of the temperatures read from the droplet, vapor, and bath thermocouples and the predicted values in the vapor at the interface (points with error bars). (b) The model used to construct the temperature profile in the vapor phase.

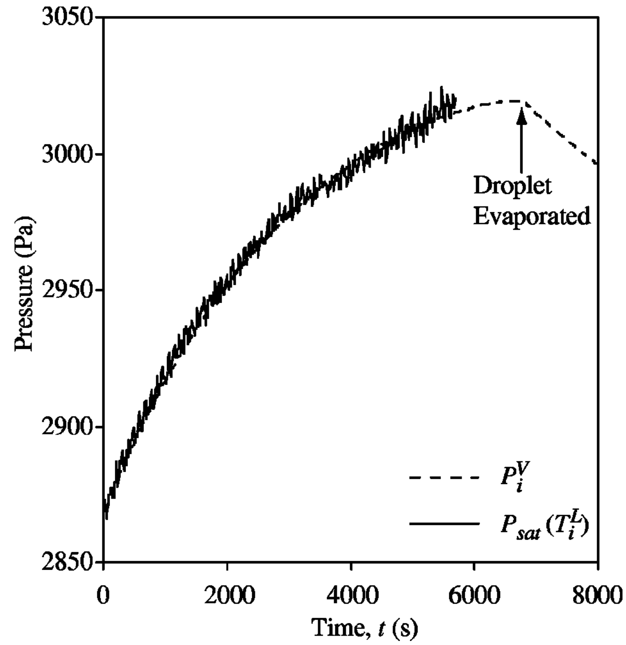

FIG. 4. The measured pressure in the vapor for test 2 and the saturation pressure corresponding to the droplet temperature. The saturation pressure curve ends at the point where some of the thermocouple bead became exposed to the vapor, and thus was no longer an indication of the liquid temperature.

the evaporation is constant, as the droplet starts and ends in the same state for each test, although the time scales are different. It is through adsorption on the solid surface that the three tests are differentiated. In a series of separate adsorption tests run on the system, it was found that the amount of mass that can adsorb on the surface increases significantly as the pressure in the system increases.[30] When the evaporation is complete, the measured pressure starts to decrease, as adsorption is the only significant factor left that affects the system pressure. This is the effect of considering a finite system.

The measured temperatures in the liquid can now be considered. One of the assumptions in the D^2 law is that the pressure in the vapor at the droplet surface is equal to the saturation pressure corresponding to the droplet surface temperature. Furthermore, the temperature in the droplet is assumed to have no spatial variation. To this end, the saturation pressure corresponding to the measured temperature in the liquid for test 2 is included in Fig. 4. The added line covers the time from a droplet diameter of 1.50 mm to just before all the liquid evaporated. For this and all subsequent calculations, thermophysical properties are taken from Ref. 32.

The pressure in the vapor phase follows the saturation pressure corresponding to the liquid temperature very closely. Any differences are covered by the experimental errors. It is therefore possible to predict the pressure in the system while the droplet is evaporating with only the measurement of the liquid temperature. Similar agreement is found for tests 1 and 3. The agreement between the two curves also gives strong support for there being no significant air content in the system. It is important to note that it is not being said that the pressure in the vapor is equal to the saturation pressure corresponding to the liquid temperature, only that experimentally, it would be impossible to distinguish between the two. This point will be important when the data is analyzed using the SRT.

It has been established that the adsorbed phase to a great extent regulates the pressure in the vapor. It now appears that the pressure in the vapor controls the droplet temperature. For test 1, where the measured vapor pressure changes very little during the evaporation due to the large amount of adsorption that can take place, the temperature in the liquid phase also changes very little. For test 3, where there is a large change in the measured vapor pressure as less adsorption takes place, there is a large change in the liquid temperature.

V. ANALYSIS AND DISCUSSION

A. Temperature discontinuity at the interface

The temperature in the liquid is assumed to be spatially uniform. Hegseth *et al.*[33] have observed Marangoni convection in evaporating methanol droplets. The resulting internal circulation would result in fluid mixing and a more uniform temperature distribution than would exist under pure conduction heat transfer. While Marangoni convection has been well documented for fluids other than water,[34,35] only recently have experiments been reported indicating that it is present in water.[8] These findings support the assumption of a uniform liquid temperature. Thus, the temperature in the liquid at the interface will taken as that measured by the droplet thermocouple, which will be denoted as T_i^L.

To calculate the temperature in the vapor at the interface, T_i^V, an approximate temperature profile will be determined in the vapor phase using the measured temperatures. The system of interest in shown in Fig. 3(b). The droplet radius is r_D (i.e., $D/2$), T_{tc}^V is the temperature measured by the vapor thermocouple and r_V is the distance between the center of the droplet and the center of the vapor thermocouple. The temperature in the vapor at the wall is assumed to be equal to the bath temperature, T^B, and the distance from the center of the droplet to this point is r_B.

To construct a temperature profile in the vapor, the various modes of heat transfer present must be considered. As discussed in Sec. IV B, there is convection associated with the radial flow of mass away from the droplet. This convection can be modeled with a radial velocity u_r. At the same time, heat is transferred by conduction against the flow of mass. While the D^2 law ignores gravitational effects, in the real flow a thermobuoyant flow is likely to develop where the cool vapor flows down the surface of the droplet and off its bottom. This component of the flow will be modeled using an polar velocity u_ϕ. The steady energy equation takes the form

$$\frac{\rho^V c_p^V}{k^V}\left(u_r\frac{dT}{dr}+\frac{u_\phi}{r}\frac{dT}{d\phi}\right)=\frac{1}{r^2}\frac{d}{dr}\left(r^2\frac{dT}{dr}\right), \tag{3}$$

where k is the thermal conductivity. Defining a dimensionless length $\overline{R}$ and temperature $\overline{T}$ as

$$\overline{R}=\frac{r}{r_V} \quad \text{and} \quad \overline{T}=\frac{T-T_i^L}{T_{tc}^V-T_i^L},$$

the energy equation can be recast as

$$\mathrm{Pe}_r\frac{d\overline{T}}{d\overline{R}}+\frac{\mathrm{Pe}_\phi}{\overline{R}}\frac{d\overline{T}}{d\phi}=\frac{1}{\overline{R}^2}\frac{d}{d\overline{R}}\left(\overline{R}^2\frac{d\overline{T}}{d\overline{R}}\right), \tag{4}$$

where Pe_r and Pe_ϕ are the radial and polar Peclet numbers, given by

$$\mathrm{Pe}_r=\frac{\rho^V c_p^V u_r r_V}{k^V} \quad \text{and} \quad \mathrm{Pe}_\phi=\frac{\rho^V c_p^V u_\phi r_V}{k^V},$$

respectively. From continuity considerations, the radial velocity will be greatest at the surface of the droplet. To assess the importance of the left side of Eq. (4), the region between the droplet and the vapor thermocouple will therefore be considered. Using an order of magnitude analysis, the left and right sides of Eq. (4) become

$$\mathrm{Pe}_r\frac{\overline{T}(\overline{R}_V)-\overline{T}(\overline{R}_D)}{\overline{R}_V-\overline{R}_D}, \quad \mathrm{Pe}_\phi\frac{\overline{T}(\overline{R}_V)-\overline{T}(\overline{R}_D)}{\pi\overline{R}}$$

and

$$\frac{1}{\overline{R}^2}[\overline{T}(\overline{R}_V)-\overline{T}(\overline{R}_D)]\frac{\overline{R}_V+\overline{R}_D}{\overline{R}_V-\overline{R}_D}.$$

The same temperature scale has been used in both directions. Physically, due to the Marangoni convection in the liquid, the droplet surface temperature will be approximately uniform, and the temperature variation in the polar direction will be smaller than that in the radial direction. Thus by choosing this temperature scale, we are considering a larger thermobuoyant convection contribution than that actually present. To assess the importance of the convection terms, we must consider the ratios

$$C_r=\frac{\mathrm{Pe}_r\overline{R}^2}{(\overline{R}_V+\overline{R}_D)} \tag{5}$$

and

$$C_\phi=\frac{\mathrm{Pe}_\phi\overline{R}(\overline{R}_V-\overline{R}_D)}{\pi(\overline{R}_V+\overline{R}_D)}, \tag{6}$$

which represent the ratios of the radial and polar convection terms to the conduction term in the energy equation. If either of these ratios is small compared to unity, the associated convection term can be neglected. Both of these ratio terms are solely functions of the position $\overline{R}$ both explicitly and implicitly (through the Peclet numbers). As mentioned, the convection effects are expected to be most significant at the droplet surface and for this reason, $\overline{R}$ is evaluated as $\overline{R}_D$. To evaluate the Peclet numbers, the properties of water vapor are evaluated at their saturation values corresponding to 26.85 °C, a typical value of T^B.

First, consider the radial term. At the droplet surface, the radial velocity can be expressed in terms of the evaporative mass flux j as

$$u_r(r_D)=\frac{j}{\rho^V}. \tag{7}$$

To calculate the mass flux, the time history of the droplet size is used. The evaporative mass flux can be expressed as

$$j=-\rho^L\frac{dr_D}{dt}. \tag{8}$$

At a given point, it is a function of the slope of the droplet size-time history. The droplet diameter as a function of time is approximately linear over small time intervals between diameters of 1.50 and 1.00 mm. The flux at a measurement point is calculated by finding the slope of the best-fit line through that point and the two points on either side of it, for a total of five points. A sample of the calculated mass fluxes for test 2 are given in Table II. For this calculation, the mass flux is chosen as the highest encountered in the evaporation tests, which is 1.38×10^{-4} kg/m^2 s (measured in test 3). The radius of the droplet in this case was 5.60×10^{-4} m. This corresponds to a radial Peclet number of 0.057, and C_r value of 0.000 84. It is therefore justifiable to neglect the radial convection term in the determination of the temperature profile.

TABLE II. A sample of the measured and calculated parameters for test 2.

r_D (mm)	r_V (mm)	T_{tc}^V (°C)	T_i^L (°C)	j (10^{-5} kg/m^2 s)	T_i^V (°C)	$T_i^V - T_i^L$ (°C)
0.74	4.03	26.46	23.43	5.31	24.30	0.87
0.71	4.06	26.49	23.54	6.12	24.39	0.85
0.69	4.08	26.54	23.63	6.12	24.63	1.00
0.67	4.10	26.57	23.72	6.12	24.76	1.04
0.65	4.12	26.58	23.81	4.90	24.74	0.93
0.63	4.15	26.57	23.84	6.12	24.60	0.76
0.60	4.18	26.60	23.90	6.94	24.71	0.81
0.58	4.20	26.61	23.95	5.31	24.69	0.74
0.57	4.24	26.61	23.98	6.12	24.61	0.63
0.54	4.33	26.67	24.02	6.94	24.99	0.97
0.51	4.43	26.66	24.07	6.12	24.75	0.68

For the polar term, corresponding to the thermobuoyant convection, an approach developed by Abramzon and Sirignano[16] is used. In their model, based on ''film theory,'' convection effects are limited to a thin vapor region surrounding the droplet. Using a Nusselt number correlation for thermobuoyant convection around an evaporating droplet given by Daif *et al.*[17] this thickness can be calculated. To examine the most extreme case, the mass flow used in the radial calculation is assumed to be flowing only in the polar direction inside this film, and we calculate the associated average velocity at the midpoint of the droplet. Using this value, the polar Peclet number is found to be 0.23, and C_ϕ evaluates to 0.0074, which we note is the most extreme case. It is therefore also justifiable to neglect the polar convection term in the determination of the vapor phase temperature profile.

To find the temperature profile in the vapor, one must then solve

$$\frac{1}{r^2}\frac{d}{dr}\left(r^2\frac{dT}{dr}\right)=0 \tag{9}$$

with the boundary conditions

$$T(r_V)=T_{tc}^V \quad \text{and} \quad T(r_B)=T^B.$$

The solution is

$$T(r)=T_{tc}^V+(T^B-T_{tc}^V)\,\frac{1/r_V-1/r}{1/r_V-1/r_B}. \tag{10}$$

As the droplet evaporates, the distance from its surface to the vapor thermocouple increases. The droplet tends to slowly move up the thermocouple wires during this time. To account for these effects, r_V has been determined separately for every calculation using the images from the experiments, based on the known distance between the two thermocouple beads and the relative location of the center of the droplet and the droplet thermocouple bead. The value of r_V varies between 3.89 and 4.46 mm. The dimension r_B is taken as the shortest distance between the droplet thermocouple and the side of the main chamber. This has been measured as 0.027 m. Due to the spherical nature of the system under consideration, and the large size of the test section compared to the droplet, the results are not sensitive to the small changes in r_B that would be brought about by the movement of the droplet. To determine T_i^V, Eq. (10) must be evaluated at the radius of the droplet. A sample of the results of these calculations for test 2 are given in Table II. Note that r_D, T_{tc}^V, T^B, and T_i^L are measured, while j, r_V, and T_i^V are calculated. To show the temperature discontinuity graphically, the predicted temperature in the vapor at the interface is included in Fig. 3(a) for droplet radii between 1.50 and 1.00 mm. The error bars are an indication of the uncertainty brought about by the temperature and length measurements.

The temperature in the vapor at the interface is found to always be higher than that in the liquid. This is consistent with the results of the previous steady evaporation experiments. There is some scatter in the data, which can be partly attributed to noise in the temperature measurement signal. Similar results are found for tests 1 and 3. In test 1, where the mass flux was lower, the temperature difference is smaller. In test 3, where the mass flux was higher, the temperature difference is larger. Using the experimental data, the largest discontinuity predicted by one approach using the CKT[20] is -6×10^{-6} °C, which is much less than the smallest predicted value, and in the opposite direction.

To try to correlate the current data with existing experimental results, the temperature discontinuity was plotted as a function of the pressure. The results are shown in Fig. 5. References 5 and 8 correspond to studies of the steady evaporation of water. For these experiments, the temperature discontinuity was measured. This was possible due to the steady nature of the evaporating interface, and the low pressures considered, which resulted in a large mean free path. Very small thermocouples were used to make the temperature measurements to within a few mean free paths of the interface. The range of the system parameters for each data set is presented in Table III. The range of the parameters is significantly different between the steady experiments and the current investigation. While the current work does not overlap with the existing results, the data follow a consistent trend. As the pressure increases, the temperature discontinuity decreases. At atmospheric pressure, it is likely that the discontinuity could not be measured.

B. Statistical rate theory analysis

The experimental results can be analyzed using the SRT, which was introduced in Sec. II. It can be used to predict that the mass flux, j, across a liquid-vapor interface at an instant in time in an isolated system will be given by[6]

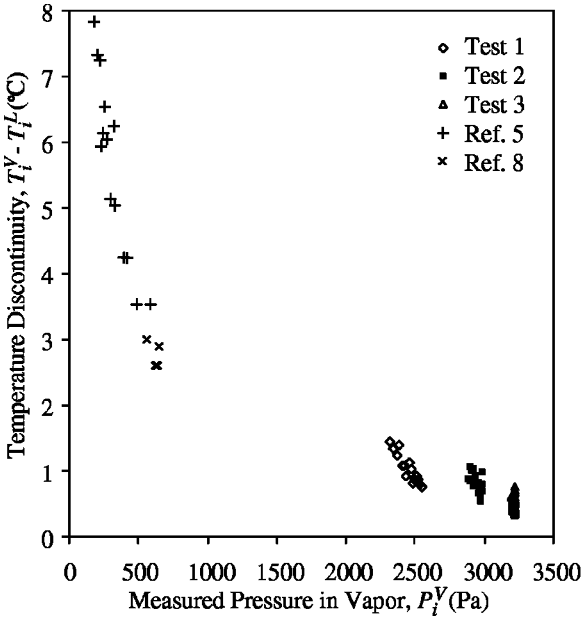

FIG. 5. A comparison of the temperature discontinuity measured in the current investigation of unsteady evaporation and previous studies of steady water evaporation.

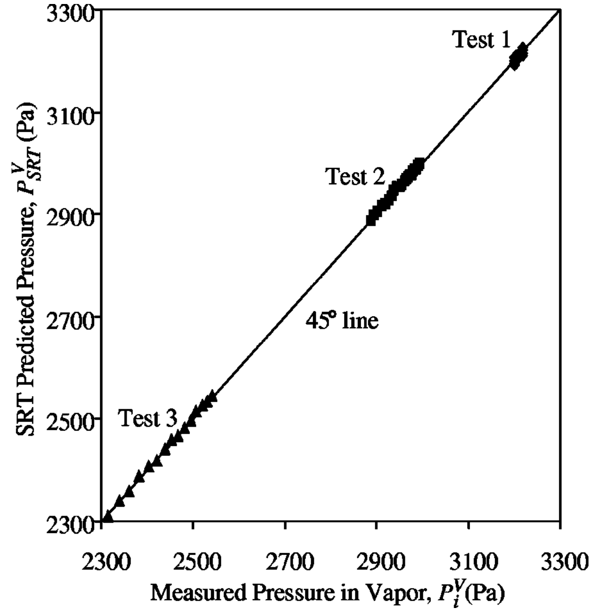

FIG. 6. The pressure in the vapor predicted by the SRT plotted against the measured pressure in the vapor. The solid line has slope of unity and would correspond to perfect agreement. The size of the data points contains the experimental error.

$$j=\frac{\eta P_{\mathrm{sat}}(T_i^L)}{\sqrt{2\pi m k_B T_i^L}}\left[\exp\left(\frac{\Delta S}{k_B}\right)-\exp\left(\frac{-\Delta S}{k_B}\right)\right], \tag{11}$$

where

$$\eta=\exp\left\{\frac{v_\infty^L(T_i^L)}{k_B T_i^L}[P_e^L-P_\infty(T_i^L)]\right\}, \tag{12}$$

$$\begin{aligned}\frac{\Delta S}{k_B}=&4\left(1-\frac{T_i^V}{T_i^L}\right)+\left(\frac{1}{T_i^V}-\frac{1}{T_i^L}\right)\sum_{l=1}^{3}\left\{\frac{\theta_l}{2}\right.\\&\left.+\frac{\theta_l}{\exp[(\theta_l/T_i^L)-1]}\right\}+\frac{v_\infty^L(T_i^L)}{k_B T_i^L}\left[P_i^V+\frac{2\gamma^{LV}}{R}\right.\\&\left.-P_\infty(T_i^L)\right]+\ln\left[\left(\frac{T_i^V}{T_i^L}\right)^4\frac{P_{\mathrm{sat}}(T_i^L)}{P_i^V}\right]-\ln\left[\frac{q_{\mathrm{vib}}(T_i^V)}{q_{\mathrm{vib}}(T_i^L)}\right],\end{aligned} \tag{13}$$

$$q_{\mathrm{vib}}(T)=\prod_{l=1}^{3}\frac{\exp[-\theta_l/(2T)]}{1-\exp(-\theta_l/T)}, \tag{14}$$

and P_e^L must satisfy

$$P_e^L-\frac{2\gamma^{LV}}{R}=P_{\mathrm{sat}}(T_i^L)\exp\left\{\frac{v_{\mathrm{sat}}^L(T_i^L)}{k_B T_i^L}[P_e^L-P_{\mathrm{sat}}(T_i^L)]\right\}. \tag{15}$$

In these equations, P_i^V is the pressure in the vapor at the interface, R is the radius of curvature of the interface, which in this case is the radius of the droplet r_D, v is specific volume, γ is surface tension, θ_l are the molecular vibrational temperatures, k_B is the Boltzmann constant, m is the molecular weight of the fluid, and the subscript sat refers to saturation conditions. Full details of the derivation and interpretation of this relation can be found in Refs. 6 and 7. The expression for the mass flux contains no fitting parameters.

Having assumed that the liquid temperature at any instant in time is uniform, T_i^L has been directly measured. The pressure in the system at any instant in time is also assumed to be uniform and as there is no significant air content, P_i^V has also been directly measured. The droplet diameter D has been measured, and thus r_D is also known. The remainder of the terms in the expression for the mass flux can be found with knowledge of the fluid and the temperatures.

It has been found that the SRT expression for j is most sensitive to the pressure in the vapor.[7] For this reason, previous investigations have tested the theory by using the experimental values of j, T_i^V, T_i^L, and r_D to predict P_i^V, and then comparing this to the experimental measurement. The same procedure is used for the current investigation. Plots of the predicted pressure from the SRT against the measured pressure for all three tests are shown in Fig. 6. The experi-

TABLE III. A comparison of the range of the temperatures, mass fluxes and radii encountered in the different investigations considered in Fig. 5 Water is the working fluid in all cases.

Data set	T_i^V (°C)	T_i^L (°C)	j (10^{-3} kg/m^2 s)	P_i^V (Pa)	R (mm)
Ref. 5	(−6.8, 3.2)	(−14.6, 0.6)	(0.25, 0.54)	(195, 596)	(3.95, 4.60)
Ref. 8	(2.4, 2.5)	(−0.4, −0.1)	(0.42, 1.06)	(560, 653)	(4.19, 7.26)
Current	(21.3, 25.7)	(19.8, 25.3)	(0.03, 0.14)	(2313, 3220)	(0.50, 0.75)

TABLE IV. A sample of the measured pressures and SRT predictions for test 2. The measured rate is $K=2.96\times10^{-4}$ mm^2/s. The collapse pressure is the difference between the pressure used in the calculations and that required to make the predicted value agree with the measured rate.

r_D (mm)	P_i^V (Pa)	P_{SRT}^V (Pa)	K_{SRT} (10^{-4} mm^2/s)	Collapse pressure, $P_{\mathrm{sat}}(T_i^L)-P^V(K_{\mathrm{SRT}}\rightarrow K_{\mathrm{meas}})$ (mPa)
0.74	2887	2885	5.94	6.1
0.71	2905	2905	5.52	5.4
0.69	2920	2920	7.68	4.7
0.67	2934	2936	7.80	3.9
0.65	2946	2952	6.12	3.0
0.63	2956	2955	3.80	2.3
0.60	2966	2967	4.14	0.8
0.58	2975	2975	3.30	0.3
0.57	2982	2982	2.16	−1.2
0.54	2989	2988	5.50	−3.1
0.51	2995	2998	2.30	−4.6

mental error is covered by the size of the data points. The solid line is at 45°, and would indicate perfect agreement. A sample of the data for test 2 is given in Table IV. The largest difference between the predictions and the measurements over the three tests (80 data points) is 9 Pa, which is within the measurement error of the pressure. The predicted pressure is always very close to the saturation pressure corresponding to the liquid temperature, but is not equal to it. The difference between the two is always less than 0.05 Pa. This difference could not be measured experimentally. The good agreement indicates that the SRT is consistent with the existence of a temperature discontinuity.

C. Predictions of the rate of evaporation

In Sec. II, the D^2 law was presented. It predicts that the droplet surface area will decrease at a constant rate K, given by Eq. (2). To compare this prediction to the experimental results, the fluid properties must be specified. As the system has only one component, all instances of the superscript G can be replaced with V, which corresponds to the pure vapor phase. The mass diffusion coefficient δ^V is then a self diffusion coefficient. From the CKT, it is predicted to be[36]

$$\delta^V=\frac{3}{8\pi d^2\rho^V}(\pi m k_B T^V)^{1/2}, \tag{16}$$

where d is the molecular diameter in the hard sphere approximation. The molecular diameter can be estimated as[37]

$$d=\left(\frac{1}{3\pi\mu^V}\sqrt{\frac{3mk_BT^V}{2}}\right)^{1/2}, \tag{17}$$

where μ is the dynamic viscosity. Combining Eqs. (16) and (17) gives

$$\delta^V=\frac{9\mu^V}{8\rho^V}\sqrt{\frac{2\pi}{3}}. \tag{18}$$

Substituting Eq. (18) into Eq. (2) gives

$$K=\frac{9\mu^V}{\rho^L}\sqrt{\frac{2\pi}{3}}\ln\left(1+\frac{c_p^V\Delta T}{h_{fg}}\right). \tag{19}$$

TABLE V. Comparison of the predictions of the D^2 law to the experiments.

Test	$\overline{K_{\mathrm{pred}}}$ (10^{-4} mm^2/s) $\Delta T=T^B-T_i^V$	$\overline{K_{\mathrm{pred}}}$ (10^{-4} mm^2/s) $\Delta T=T^B-T_i^L$	K_{meas} (10^{-4} mm^2/s)
1	0.94 (+0.15, −0.23)	1.42 (+0.09, −0.06)	1.49
2	2.02 (+0.29, −0.32)	2.75 (+0.34, −0.23)	2.96
3	4.44 (+0.42, −0.32)	5.36 (+0.78, −0.50)	5.64

For the subsequent calculations, μ^V and c_p^V are evaluated at the saturation conditions corresponding to a reference temperature T_{ref} recommended by Abramzon and Sirignano as[16]

$$T_{\mathrm{ref}}=T_i^V+\tfrac{1}{3}(T^B-T_i^V). \tag{20}$$

The liquid density and the latent heat of vaporization are evaluated at the saturation conditions corresponding to the measured droplet temperature. The temperature difference in Eq. (19) is specified in the D^2 law as the difference between the ambient temperature and the temperature at the surface of the droplet. The temperature of the water bath, T^B, is taken as the ambient temperature. It has been found that there is a temperature discontinuity at the droplet surface, and a question arises as to which temperature to use: T_i^L or T_i^V.

In following the logic of the D^2 law, which is a gas phase model, one would take the temperature difference as $T^B-T_i^V$. For each of the three tests, K has been predicted at each of the points where the droplet size was measured. Note that as the properties and the temperature difference in Eq. (19) change during the evaporation process, the predicted value of K will also change. When this is done, the D^2 law underpredicts the average rate of evaporation by 21%–37%.

However, if the temperature difference is calculated using T_i^L in the expression for ΔT, i.e., taking the temperature discontinuity into account, the difference between the measured and average predicted rates is at most 7%. The measured rate falls within the range of the predicted values for all three tests. The results, along with the experimental measurements of K, are presented in Table V. Inclusion of the conditions at the surface have led to a much better prediction of the rate of evaporation. While the D^2 law assumes that the rate limiting process is diffusion in the gas phase, these results indicate that the interface kinetics play an important, if not dominant role in the current experiments.

A prediction of the parameter K from the D^2 law can also be made using the SRT. The time rate of change of the square of the droplet diameter can be expressed as

$$-\frac{dD^2}{dt}=-8r_d\frac{dr_d}{dt}. \tag{21}$$

With the definition of mass flux from Eq. (8), Eq. (21) becomes

$$-\frac{dD^2}{dt}=-\frac{8r_dj}{\rho^L}. \tag{22}$$

The left side of Eq. (22) has been measured, and is a constant for each of the evaporation experiments. The right side can be evaluated by using Eq. (11) to predict the value of j, and using the measured droplet radius and properties at each of the measurement points.

As discussed, the SRT expression for the mass flux is very sensitive to the pressure in the vapor. If the right side of Eq. (22) is evaluated using the measured pressures, the results show a large scatter. It has been observed that the measured pressure in the vapor is very close to the saturation pressure corresponding to the liquid temperature.[8] With this approximation, the mass flux in Eq. (22) was evaluated by assuming that

$$P_i^V = P_{\mathrm{sat}}(T_i^L). \tag{23}$$

A sample of the results of these calculations for test 2 are presented in Table IV.

Also included in this table is the ''collapse pressure.'' This is defined as the difference between the pressure used in the calculation, Eq. (23), and the pressure that would make the predicted rate agree with that measured. The collapse pressure is on the order of millipascals. This is extremely small and could not be resolved experimentally. Similar results were found for tests 1 and 3. While the range of the predicted values of the rate of evaporation from the SRT is large, this is compensated for by the extreme sensitivity to the pressure. In that light, the predicted values can be considered to be quite good. The fact that an interface kinetics model that is consistent with a temperature discontinuity is able to give a reasonable prediction of the rate of evaporation, combined with the observed effect of including the discontinuity in the D^2 law, leads to the conclusion that the rate limiting process in the current experiments is the interface kinetics.

VI. CONCLUSION

The results of a series of droplet evaporation experiments have been found to be consistent with previous experimental work and SRT predictions. As shown in Fig. 3(a) and Table II, a temperature discontinuity has been found to exist at the liquid-vapor interface, with the temperature always being higher on the vapor side. This phenomenon is interpreted as an indication that the higher energy molecules are evaporating.[8] The discontinuity is in the opposite direction to and six orders of magnitude larger in size than the predictions of the CKT.[20] The magnitude and direction of the discontinuity are in agreement with the results of previous steady evaporation experiments.[5–8] Using the SRT, the pressure in the vapor has been predicted to within the experimental uncertainty for all cases considered (see Fig. 6 and Table IV). This indicates that the SRT is consistent with the observed temperature discontinuity. It is emphasized that the SRT calculations were performed without any fitting parameters.

The qualitative trend of the D^2 law is consistent with the observations, but it is unable to give a good numerical prediction of the rate of evaporation. However, when the temperature discontinuity is taken into account in the D^2 law, it gives a more accurate prediction, as shown in Table V. When taking into account its extreme pressure sensitivity, the SRT is found to give a reasonable prediction of the rate of evaporation (see Table IV). The results suggest that the rate limiting process in the current experiments is the interface kinetics, and not diffusion in the gas phase, as is assumed in the D^2 law.

ACKNOWLEDGMENTS

This work was supported by the Natural Sciences and Engineering Research Council of Canada, the Canadian Space Agency, and Ontario Hydro Technologies.

1. G. A. E. Godsave, *Fourth Symposium (International) on Combustion* (Williams and Wilkins, Baltimore, 1953), pp. 818–830.
2. D. B. Spalding, *Fourth Symposium (International) on Combustion* (Williams and Wilkins, Baltimore, 1953), pp. 847–864.
3. M. Goldsmith and S. S. Penner, Jet Propul. **24**, 245 (1954).
4. H. Wise, J. Lorell, and B. J. Wood, *Fifth Symposium (International) on Combustion* (Reinhold, New York, 1955), pp. 132–141.
5. G. Fang and C. A. Ward, Phys. Rev. E **59**, 417 (1999).
6. C. A. Ward and G. Fang, Phys. Rev. E **59**, 429 (1999).
7. G. Fang and C. A. Ward, Phys. Rev. E **59**, 441 (1999).
8. C. A. Ward and D. Stanga, Phys. Rev. E **64**, 051509 (2001).
9. C. A. Ward, J. Chem. Phys. **67**, 229 (1977).
10. C. A. Ward, R. D. Findlay, and M. Rizk, J. Chem. Phys. **76**, 5599 (1982).
11. C. A. Ward, J. Chem. Phys. **79**, 5605 (1983).
12. C. K. Law, Prog. Energy Combust. Sci. **8**, 171 (1982).
13. W. A. Sirignano, J. Fluids Eng. **115**, 345 (1993).
14. T. Elperin and B. Krasovitov, Int. J. Heat Mass Transf. **38**, 409 (1995).
15. P. L. C. Lage, C. M. Hackenberg, and R. H. Rangel, Int. J. Heat Mass Transf. **36**, 3731 (1993).
16. B. Abramzon and W. A. Sirignano, Int. J. Heat Mass Transf. **32**, 1605 (1989).
17. A. Daif, M. Bouaziz, X. Chesneau, and A. Ali Cherif, Exp. Therm. Fluid Sci. **18**, 282 (1999).
18. J. Margerit and O. Sero-Guillaume, Int. J. Heat Mass Transf. **39**, 3887 (1996).
19. S. M. Ghiaasiaan and D. Luo, Int. J. Heat Mass Transf. **37**, 461 (1994).
20. J. B. Young, Int. J. Heat Mass Transf. **34**, 1649 (1991).
21. Y. I. Yalamov, E. R. Shchukin, and E. I. Alekhin, High Temp. **28**, 184 (1990).
22. G. Fang, Ph.D. thesis, Department of Mechanical and Industrial Engineering, University of Toronto, 1998.
23. J. A. W. Elliott and C. A. Ward, Stud. Surf. Sci. Catal. **104**, 285–333 (1995).
24. J. A. W. Elliott and C. A. Ward, J. Chem. Phys. **106**, 5667 (1997).
25. J. A. W. Elliott and C. A. Ward, J. Chem. Phys. **106**, 5677 (1997).
26. J. A. W. Elliott and C. A. Ward, Langmuir **13**, 951 (1997).
27. C. A. Ward and M. Elmoselhi, Surf. Sci. **176**, 457 (1986).
28. F. K. Skinner, C. A. Ward, and B. L. Bardakjian, Biophys. J. **65**, 618 (1993).
29. M. Dejmek and C. A. Ward, J. Chem. Phys. **108**, 8698 (1998).
30. A. J. H. McGaughey, M. A. Sc. thesis, Department of Mechanical and Industrial Engineering, University of Toronto, 2000.
31. http://rsb.info.nih.gov/nih-image/.
32. M. J. Moran and H. N. Shapiro, *Fundamentals of Engineering Thermodynamics* (Wiley, New York, 1995), p. 723; F. P. Incropera and D. P. Dewitt, *Fundamentals of Heat and Mass Transfer* (Wiley, New York, 1996), p. 846.
33. J. J. Hegseth, N. Rashidnia, and A. Chai, Phys. Rev. E **54**, 1640 (1996).
34. A-T. Chai and N. Zhang, Exp. Heat Transfer **11**, 187 (1998).
35. M. Assenheimer and V. Steinberg, Phys. Rev. Lett. **70**, 3888 (1993).
36. R. D. Present, *Kinetic Theory of Gases* (McGraw-Hill, New York, 1958), p. 55.
37. R. D. Present, *Kinetic Theory of Gases* (McGraw-Hill, New York, 1958), p. 44.